

Learning-Based Joint Antenna Selection and Precoding Design for Cell-Free MIMO Networks

Liangzhi Wang, *Graduate Student Member, IEEE*, Chen Chen, *Member, IEEE*, Carlo Fischione, *Senior Member, IEEE*, and Jie Zhang, *Senior Member, IEEE*

Abstract—This paper considers a downlink cell-free multiple-input multiple-output (MIMO) network in which multiple multi-antenna base stations (BSs) serve multiple users via coherent joint transmission. In order to reduce the energy consumption by radio frequency components, each BS selects a subset of antennas for downlink data transmission after estimating the channel state information (CSI). We aim to maximize the sum spectral efficiency by jointly optimizing the antenna selection and precoding design. To alleviate the fronthaul overhead and enable real-time network operation, we propose a distributed scalable machine learning algorithm. In particular, at each BS, we deploy a convolutional neural network (CNN) for antenna selection and a graph neural network (GNN) for precoding design. Different from conventional centralized solutions that require a large amount of CSI and signaling exchange among the BSs, the proposed distributed machine learning algorithm takes only locally estimated CSI as input. With well-trained learning models, it is shown that the proposed algorithm significantly outperforms the distributed baseline schemes and achieves a sum spectral efficiency comparable to its centralized counterpart.

Index Terms—Cell-free MIMO, sum spectral efficiency, antenna selection, precoding, machine learning.

I. INTRODUCTION

MASSIVE multiple-input multiple-output (MIMO) has been one of the most promising technologies in the fifth generation (5G) and beyond wireless communication networks [1], [2]. A massive MIMO base station (BS) is equipped with a large number of antenna elements, which allows it to spatially multiplex multiple users over the same time-frequency resource. However, the conventional cellular massive MIMO architecture cannot achieve uniform coverage at high spectral efficiency; the cell-edge users suffer from long transmission distances and severe inter-cell interference [3]. To

this end, a new post-cellular network infrastructure, termed as cell-free MIMO, was proposed in [4]. In cell-free MIMO networks, the BSs are connected to a central processing unit (CPU) or an edge-cloud processor via high-speed fronthaul links [5]. All the BSs cooperatively serve the users by coherent joint transmission, eliminating cell-boundaries and inter-cell interference. This enables an improvement in both spectral efficiency and energy efficiency [6]. On the other hand, the number of radio frequency (RF) chains increases with the number of antennas, which leads to escalating hardware cost and energy consumption [7]. In this regard, antenna selection can be employed to reduce the energy consumption by activating only the antennas that contribute the most to the system throughput [8].

Antenna selection has been extensively investigated in massive MIMO systems [9]–[13]. An exhaustive search for the optimal subset of antennas is generally computationally prohibitive. In [9], the authors considered zero-forcing precoding and converted the antenna selection problem into a convex optimization problem by relaxing the integer constraints. In [10], antenna selection schemes based on genetic algorithms (GAs) were developed, which were shown to achieve almost the same throughput as exhaustive search. GA-based antenna selection was also adopted in [14] to maximize the energy efficiency of a extra-large scale MIMO system. The authors in [11] proposed to apply stochastic gradient descent in joint antenna selection and user scheduling to maximize the energy efficiency of a single-cell MIMO system. In [12], the authors investigated limited-resolution analog-to-digital converters and digital-to-analog converters, and developed two quantization-aware antenna selection algorithms for downlink and uplink transmissions, respectively. Recently, antenna selection in a full-duplex cell-free network was addressed centrally by an elite preservation GA at the CPU [13]. The antenna selection schemes proposed in these works require iterative optimization, resulting in unacceptable computational burden.

An alternative solution is to develop low-complexity schemes utilizing the recent advances of machine learning [15], [16]. Deep neural networks (DNNs) are able to approximate the complex mapping relationships between the time-varying channel conditions and the desired system configurations. The computational complexity is shifted to the offline training phase, allowing real-time online implementation. In [17], [18], deep learning was employed in channel estimation tasks of massive MIMO systems. In [19], [20], learning-based solutions were developed to jointly configure the transmit precoding at the multi-antenna BS and the phase

Manuscript received xxx; revised xxx; accepted xxx. Date of publication xxx; date of current version xxx. The work of Liangzhi Wang and Jie Zhang was supported in part by the U.K. Engineering and Physical Sciences Research Council under Grant 101086219. The work of Chen Chen and Carlo Fischione was supported in part by the KTH Digital Future research center. The review of this paper was coordinated by xxx.

Liangzhi Wang is with the Department of Electronic and Electrical Engineering, University of Sheffield, Sheffield, S10 2TN, UK (e-mail: lwang85@sheffield.ac.uk).

Chen Chen and Carlo Fischione are with the School of Electrical Engineering and Computer Science, KTH Royal Institute of Technology, Stockholm, Sweden (e-mail: {chch2, carlofi}@kth.se).

Jie Zhang is with the Department of Electronic and Electrical Engineering, University of Sheffield, Sheffield, S10 2TN, UK, and also with Ranplan Wireless Network Design Ltd., Cambridge, CB23 3UY, UK (e-mail: jie.zhang@sheffield.ac.uk).

Color versions of one or more of the figures in this paper are available online at <http://ieeexplore.ieee.org>.

Digital Object Identifier xxx

shifts at the intelligent reflecting surface. In the context of a cell-free MIMO network with single-antenna BSs, the joint channel estimation and beamforming was addressed in [21] by developing model-driven deep learning solution. In [22], the BS-user association was optimized by deep reinforcement learning (DRL) to maximize the uplink energy efficiency in a user-centric cell-free MIMO network assuming maximum ratio combining. Deep learning was exploited in uplink and downlink power control of a cell-MIMO network in [23] and [24], respectively. In particular, distributed DNNs were developed in [24] to approximate the desired power allocation coefficients using only local inputs determined by large-scale fading coefficients.

Machine learning has also found applications in antenna selection problems [25]–[29]. In the context of single-cell MIMO system, the authors in [25] modelled antenna selection as a multiclass-classification problem, which was solved by k -nearest neighbors and support vector machine algorithms. Aiming to minimize the bit error rate, the authors in [26] proposed decision tree and multi-layer perceptron (MLP) based schemes for antenna selection, taking imperfect channel state information (CSI) as input. The proposed schemes were validated via practical measurements on MIMO test-beds. In [27], an MLP was applied to antenna selection, while the precoding was optimized based on an iterative optimization algorithm. In [28], two convolutional neural networks (CNNs) were developed for antenna selection and precoding design, respectively. The CNNs were further quantized to be applicable to low-memory devices. In [29], the authors considered a cell-free MIMO scenario using conjugate beamforming. A centralized DRL-based antenna selection algorithm was developed taking the global CSI as input.

To the best of our knowledge, the joint precoding and antenna selection in cell-free MIMO networks has not been investigated yet. The main challenges of cell-free MIMO network architecture are the intensive CSI and signaling exchange over fronthaul links and the computational burden of signal processing. To reduce the fronthaul overhead of information exchange and computational complexity of joint optimization, distributed and real-time solutions are preferred. The existing centralized antenna selection and precoding schemes are not applicable in cell-MIMO scenarios. In this paper, we novelly propose a fully distributed machine learning-based algorithm for joint antenna selection and precoding design. The main contributions of this work are summarized as follows:

- First, we investigate a multi-user cell-free MIMO network and formulate a joint antenna selection and precoding design problem to maximize the downlink sum spectral efficiency, which accounts for realistic pilot-based channel estimation, subject to the transmission power budget at each BS.
- Second, we develop a distributed graph neural network (GNN)-based precoding algorithm, where each BS deploys a GNN, using only local CSI estimate of selected antennas as input. The GNNs are trained centrally at the CPU to maximize the sum spectral efficiency utilizing global CSI estimates. The well-trained GNNs can adapt to dynamic channel conditions and an arbitrarily selected

subset of antennas.

- Third, we generate training datasets for antenna selection using iterative search with the aid of the well-trained GNNs. We develop a distributed CNN for each BS to capture the mapping relationship between the local CSI estimate and the selected antenna subset.
- Finally, we perform extensive simulations to demonstrate that the proposed fully distributed joint CNN-based antenna selection and GNN-based precoding algorithm achieves a sum spectral efficiency close to its centralized counterpart by a much lower computational complexity.

The rest of this paper is organized as follows. Section II introduces the system model and problem formulation. In Section III, we describe the proposed distributed GNN-based algorithm in detail, which is used for precoding design. The proposed distributed CNN-based antenna selection algorithm is detailed in Section IV. In Section V, simulation results are presented to compare different schemes in terms of sum spectral efficiency. Finally, the major conclusions are provided in Section VI.

Notations: In this paper, italic letters, boldface lower-case letters, and boldface uppercase letters represent scalars, vectors, and matrices, respectively. \mathbf{V}^T , \mathbf{V}^H , and \mathbf{V}^* denote the transpose, conjugate transpose, and conjugate of a matrix \mathbf{V} , respectively. $\mathbb{E}\{\cdot\}$ is the statistical expectation and $\text{Tr}(\cdot)$ is the trace operation. $\|\cdot\|_F$ represents the Frobenius norm. $\mathcal{N}_{\mathbb{C}}(\mathbf{0}, \mathbf{R})$ denotes the distribution of a multivariate circularly symmetric complex Gaussian variable with zero mean and covariance matrix \mathbf{R} . \mathbf{I}_N represents a $N \times N$ identity matrix. $\mathbb{C}^{M \times N}$ and $\mathbb{R}^{M \times N}$ represent the space of complex-valued and real-valued matrices, respectively. $[\mathbf{V}]_{i,j}$ denotes the (i, j) -th element of a matrix \mathbf{V} and $[\mathbf{v}]_i$ denotes the i -th element of a vector \mathbf{v} .

II. SYSTEM MODEL AND PROBLEM FORMULATION

As shown in Fig. 1, we consider a multi-user downlink cell-free MIMO network, which consists of one CPU, K single-antenna users and I multi-antenna BSs. Each BS is equipped with N antennas. The index sets of users and BSs are represented by $\mathcal{K} = \{1, 2, \dots, K\}$ and $\mathcal{I} = \{1, 2, \dots, I\}$, respectively. We assume that the BS antenna spacing is adequate such that the channels between the BS antennas and an arbitrary user are uncorrelated [30]. The small-scale fading is assumed to follow Rayleigh distribution. Accordingly, the channel from user k to BS i is denoted by $\mathbf{h}_{i,k} \sim \mathcal{N}_{\mathbb{C}}(\mathbf{0}, \beta_{i,k} \mathbf{I}_N)$, where $\beta_{i,k}$ represents the large-scale path loss.

The CPU and BSs are connected by error-free front-haul links. Conventional centralized operation optimizes the precoding vectors at the CPU by collecting the global instantaneous CSI, which leads to a heavy front-haul overhead. In this paper, we develop efficient distributed algorithms that enable the BSs to select antenna subsets and design precoding vectors only according to their locally estimated CSI. In this way, no CSI is transmitted through the front-haul links but only uplink and downlink data.

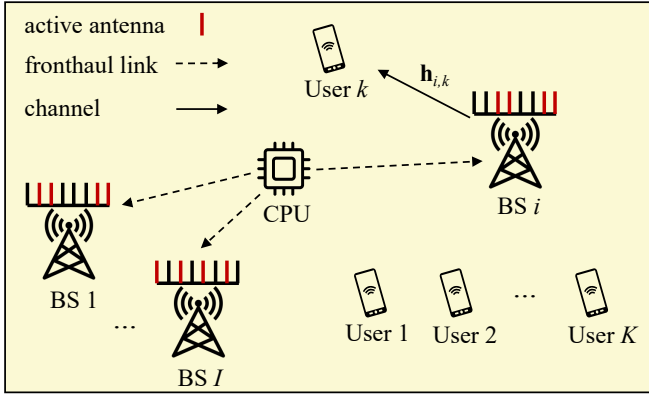


Fig. 1. An illustration of the downlink cell-free MIMO network.

A. Channel Estimation

We consider the widely-used block fading channel model where the channels are static and frequency-flat in a coherence block with τ_c time-frequency samples. Time-division duplex (TDD) protocol is adopted for channel estimation and data transmission. As shown in Fig. 2, a coherence block is divided into three phases: τ_p samples for uplink pilot transmission, τ_u samples for uplink data transmission and τ_d samples for downlink data transmission. We assign an uplink pilot signal $\phi_k \in \mathbb{C}^{\tau_p \times 1}$ to user k , $\|\phi_k\|^2 = \tau_p, \forall k \in \mathcal{K}$. We further assume that $\tau_p \geq K$ and $\phi_k^H \phi_{k'} = 0, \forall k \neq k'$. During the uplink pilot transmission phase, the received signal $\mathbf{Y}_i^p \in \mathbb{C}^{N \times \tau_p}$ at BS i is given by

$$\mathbf{Y}_i^p = \sqrt{P_{\text{ul}}} \sum_{k=1}^K \mathbf{h}_{i,k} \phi_k^H + \mathbf{N}_i^p, \quad (1)$$

where P_{ul} is the uplink pilot transmit power and $\mathbf{N}_i^p \in \mathbb{C}^{N \times \tau_p}$ is the complex Gaussian noise matrix with i.i.d. entries $\mathcal{N}_{\mathbb{C}}(0, \delta^2)$. Then BS i correlates \mathbf{Y}_i^p with ϕ_k and obtains

$$\begin{aligned} \mathbf{y}_{i,k}^p &= \sqrt{P_{\text{ul}}} \mathbf{h}_{i,k} \phi_k^H \phi_k + \sqrt{P_{\text{ul}}} \sum_{k' \in \mathcal{K}, k' \neq k} \mathbf{h}_{i,k'} \phi_{k'}^H \phi_k + \mathbf{N}_i^p \phi_k \\ &= \sqrt{P_{\text{ul}}} \tau_p \mathbf{h}_{i,k} + \mathbf{N}_i^p \phi_k, \end{aligned} \quad (2)$$

where $\mathbf{N}_i^p \phi_k \sim \mathcal{N}_{\mathbb{C}}(\mathbf{0}, \delta^2 \tau_p \mathbf{I}_N)$. The linear minimum-mean-square-error (LMMSE) estimate of $\mathbf{h}_{i,k}$ is given by

$$\hat{\mathbf{h}}_{i,k} = \sqrt{P_{\text{ul}}} \tau_p \beta_{i,k} \mathbf{Z}_{i,k}^{-1} \mathbf{y}_{i,k}^p = \frac{\sqrt{P_{\text{ul}}} \beta_{i,k} \mathbf{y}_{i,k}^p}{P_{\text{ul}} \tau_p \beta_{i,k} + \delta^2}, \quad (3)$$

where $\mathbf{Z}_{i,k} = \mathbb{E} \left\{ \mathbf{y}_{i,k}^p \left(\mathbf{y}_{i,k}^p \right)^H \right\} = P_{\text{ul}} \tau_p^2 \beta_{i,k} \mathbf{I}_N + \delta^2 \tau_p \mathbf{I}_N$.

The channel estimation error of $\mathbf{h}_{i,k}$ is given by $\tilde{\mathbf{h}}_{i,k} = \mathbf{h}_{i,k} - \hat{\mathbf{h}}_{i,k}$ with correlation matrix

$$\mathbf{C}_{i,k} = \beta_{i,k} \mathbf{I}_N - P_{\text{ul}} \tau_p^2 \beta_{i,k}^2 \mathbf{Z}_{i,k}^{-1} = \left(\beta_{i,k} - \frac{P_{\text{ul}} \tau_p \beta_{i,k}^2}{P_{\text{ul}} \tau_p \beta_{i,k} + \delta^2} \right) \mathbf{I}_N. \quad (4)$$

B. Antenna Selection

In each coherence block, we select a M -out-of- N subset of antennas as active antennas for data transmission at each

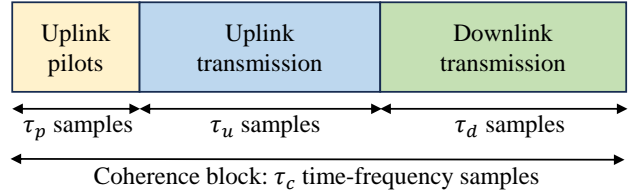


Fig. 2. An illustration of the TDD protocol.

BS. Denote the selected subset of antennas at BS i by $\mathcal{A}_i = \{a_{i,1}, a_{i,2}, \dots, a_{i,M}\}$, where $a_{i,m} \in \{1, 2, \dots, N\}$. The number of all the possible antenna subsets at BS i is $C_i = \binom{N}{M}$. Then, the channel from user k to the active antennas at BS i is given by

$$\mathbf{h}_{i,k,\mathcal{A}_i} = \left[h_{i,k,a_{i,1}}, h_{i,k,a_{i,2}}, \dots, h_{i,k,a_{i,M}} \right]^T \in \mathbb{C}^{M \times 1}, \quad (5)$$

where $h_{i,k,a_{i,m}}$ denotes the channel between antenna $a_{i,m}$ at BS i and user k . Let $\mathcal{A} = \{\mathcal{A}_1, \mathcal{A}_2, \dots, \mathcal{A}_I\}$ represent the global antenna subset in the cell-free MIMO network. The number of all the possible global antenna selection strategies is computed by $C = \prod_{i=1}^I C_i = \binom{N}{M}^I$.

In a cell-free MIMO network, each of the users is served by all the multi-antenna BSs simultaneously over the same time-frequency resource. Thus, the received signal at user k can be expressed as

$$\begin{aligned} y_k &= \underbrace{\sum_{i \in \mathcal{I}} \hat{\mathbf{h}}_{i,k,\mathcal{A}_i}^H \mathbf{w}_{i,k} s_k}_{\text{the desired signal}} + \underbrace{\sum_{i \in \mathcal{I}} \sum_{k' \in \mathcal{K}, k' \neq k} \hat{\mathbf{h}}_{i,k,\mathcal{A}_i}^H \mathbf{w}_{i,k'} s_{k'}}_{\text{the interference signal}} \\ &+ \underbrace{\sum_{i \in \mathcal{I}} \sum_{k' \in \mathcal{K}} \tilde{\mathbf{h}}_{i,k,\mathcal{A}_i}^H \mathbf{w}_{i,k'} s_{k'}}_{\text{the channel estimation errors}} + \underbrace{n_k}_{\text{the noise}}, \end{aligned} \quad (6)$$

where $n_k \sim \mathcal{N}_{\mathbb{C}}(0, \delta^2)$ denotes the additive white Gaussian noise at user k , $\mathbf{w}_{i,k} \in \mathbb{C}^{M \times 1}$ represents the beamforming vector from BS i to user k , and s_k is the required data symbol of user k . $\hat{\mathbf{h}}_{i,k,\mathcal{A}_i}$ and $\tilde{\mathbf{h}}_{i,k,\mathcal{A}_i}$ are the LMMSE estimate and estimation error of $\mathbf{h}_{i,k,\mathcal{A}_i}$, respectively.

Due to the channel estimation error, it is difficult to obtain an accurate expression of the downlink spectral efficiency. Following the existing works [31], [32], we treat the channel estimation error as Gaussian noise and adopt a lower bound of the downlink spectral efficiency as follows

$$R_k(\mathcal{A}, \mathbf{w}_k) = \frac{\tau_d}{\tau_c} \log_2(1 + \text{SINR}_k(\mathcal{A}, \mathbf{w}_k)), \quad (7)$$

where the instantaneous effective signal-to-interference-and-noise ratio (SINR) is given by

$$\begin{aligned} \text{SINR}_k(\mathcal{A}, \mathbf{w}_k) &= \frac{|\hat{\mathbf{h}}_{k,\mathcal{A}}^H \mathbf{w}_k|^2}{\sum_{k' \in \mathcal{K}, k' \neq k} |\hat{\mathbf{h}}_{k,\mathcal{A}}^H \mathbf{w}_{k'}|^2 + \sum_{k' \in \mathcal{K}} \mathbf{w}_{k'}^H \mathbf{C}_{k',\mathcal{A}} \mathbf{w}_{k'} + \delta^2}, \end{aligned} \quad (8)$$

where $\hat{\mathbf{h}}_{k,\mathcal{A}} = [\hat{\mathbf{h}}_{1,k,\mathcal{A}_1}^T, \hat{\mathbf{h}}_{2,k,\mathcal{A}_2}^T, \dots, \hat{\mathbf{h}}_{I,k,\mathcal{A}_I}^T]^T$, $\tilde{\mathbf{h}}_{k,\mathcal{A}} = [\tilde{\mathbf{h}}_{1,k,\mathcal{A}_1}^T, \tilde{\mathbf{h}}_{2,k,\mathcal{A}_2}^T, \dots, \tilde{\mathbf{h}}_{I,k,\mathcal{A}_I}^T]^T$, $\mathbf{w}_k = [\mathbf{w}_{1,k}^T, \mathbf{w}_{2,k}^T, \dots, \mathbf{w}_{I,k}^T]^T$, and $\mathbf{C}_{k,\mathcal{A}} = \text{diag}(\mathbf{C}_{1,k,\mathcal{A}_1}, \mathbf{C}_{2,k,\mathcal{A}_2}, \dots, \mathbf{C}_{I,k,\mathcal{A}_I})$ with

$$\begin{aligned} \mathbf{C}_{i,k,\mathcal{A}_i} &= \mathbb{E} \left\{ \tilde{\mathbf{h}}_{i,k,\mathcal{A}_i} (\tilde{\mathbf{h}}_{i,k,\mathcal{A}_i})^H \right\} \\ &= \left(\beta_{i,k} - \frac{P_{\text{ul}} \tau_p \beta_{i,k}^2}{P_{\text{ul}} \tau_p \beta_{i,k} + \delta^2} \right) \mathbf{I}_M. \end{aligned} \quad (9)$$

C. Problem Formulation

In this paper, we aim to maximize the sum spectral efficiency by jointly optimizing the antenna selection strategy \mathcal{A} and the precoding vectors $\{\mathbf{w}_k | \forall k \in \mathcal{K}\}$ at the BSs. Mathematically, the optimization problem can be formulated as follows

$$\max_{\mathcal{A}, \{\mathbf{w}_k\}} \sum_{k \in \mathcal{K}} R_k(\mathcal{A}, \mathbf{w}_k) \quad (10)$$

$$\text{s.t.} \quad \sum_{k \in \mathcal{K}} \text{Tr}(\mathbf{w}_{i,k} \mathbf{w}_{i,k}^H) = P_{\text{max}}, \forall i \in \mathcal{I}, \quad (10a)$$

where P_{max} is the maximum transmit power per BS. The joint optimization problem is a mixed integer non-convex optimization problem. Note that the precoding vectors are closely related to active antennas. Specifically, precoding vectors are designed for a certain, predetermined active antenna subset.

In this paper, we propose to solve the optimization problem using distributed machine learning algorithms. More specifically, we first propose a distributed GNN-based precoding scheme to optimize the precoding vectors for an arbitrary given antenna selection strategy, as detailed in Section III. Subsequently, in Section IV, we apply the well-trained GNNs to generate datasets for training CNN models that can be used to predict the optimal antenna selection strategy.

III. PROPOSED DISTRIBUTED GNN-BASED PRECODING

Conventional centralized precoding approaches such as centralized MMSE and centralized iterative optimization require the CPU to collect the global CSI and determine the precoding vectors for all the BSs, and then transmit the precoding vectors to each BS through the front-haul links. This process requires a large amount of information exchange, leading to a heavy fronthaul overhead. On the other hand, the existing distributed precoding schemes such as Maximum ratio transmission (MRT) and distributed MMSE suffer from the limited interference cancellation ability of a single BS. To this end, in this section, we develop a fully distributed precoding algorithm based on GNNs that can achieve similar sum spectral efficiency as centralized approaches. The GNNs are trained offline in a centralized manner at the CPU and downloaded by the BSs for online use in a distributed manner. Each BS is able to design its precoding vectors using the well-trained GNN only according to its locally estimated CSI.

A. Graph Construction

GNN is a class of neural network models for processing graph-structured data. A graph \mathcal{G} typically consists of node

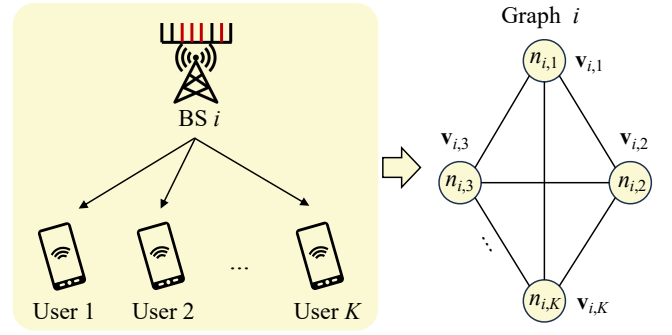


Fig. 3. An illustration of Graph i . It is a fully connected undirected graph, where node $n_{i,k}$ represents user k , and $\mathbf{v}_{i,k}$ is its feature vector.

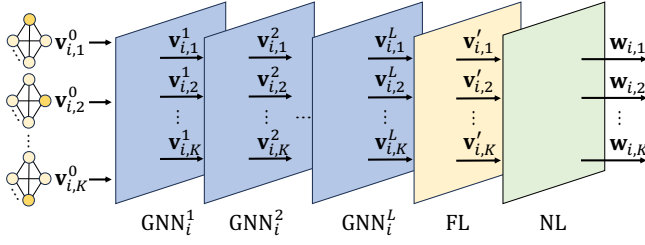
set \mathcal{N} and edge set \mathcal{E} . Each node has its own attributes that are used to store feature information such as node identity. Edges record information that describes the relationship between nodes. Edges can be directed, which means that the information transfer between nodes is unidirectional. When the information transfer between nodes is bidirectional, the edges are undirected. The connected relation between nodes can be easily represented by the adjacency matrix \mathbf{A} with main diagonal elements being zero. When node k is connected to node k' by an undirected edge, $[\mathbf{A}]_{k,k'} = [\mathbf{A}]_{k',k} = 1$; when node k and k' are not connected, $[\mathbf{A}]_{k,k'} = [\mathbf{A}]_{k',k} = 0$.

This paper aims to deploy a GNN at each BS for designing the precoding vectors. As shown in Fig. 3, graph i , $\forall i \in \mathcal{I}$, is constructed from the subnetwork consisting of BS i and all the users. Let $\mathcal{G}_i = (\mathcal{N}_i, \mathcal{E}_i)$ denote graph i , where $\mathcal{N}_i = \{n_{i,1}, \dots, n_{i,K}\}$ represents the set consisting of all user nodes and \mathcal{E}_i is the set of edges. Specifically, graph i is constructed as a fully connected undirected graph, i.e., there is an undirected connectivity between any two nodes. Hence, the adjacency matrix of graph i can be described as: $[\mathbf{A}_i]_{k,k'} = [\mathbf{A}_i]_{k',k} = 1, \forall k \neq k'$. Denote $\mathcal{V}_i = \{\mathbf{v}_{i,1}, \dots, \mathbf{v}_{i,K}\}$ as the set consisting of the feature vectors, where $\mathbf{v}_{i,k}$ is the feature vector used to characterize $n_{i,k}$.

We adopt spatial graph convolutional networks to update the feature vectors [33]. To sufficiently learn the inter-node relationships, each layer of the GNN performs convolution operations which amalgamate information from object nodes and their neighboring nodes to update the feature vectors. The feature vector update will be elaborated in the next subsection. We train the GNNs using unsupervised learning, bypassing the time-consuming step of dataset generation. Compared to other deep learning networks, GNNs can handle inter-user interference better in the precoding design [19].

B. Structure of the Proposed GNNs

The structure of GNN i , $\forall i \in \mathcal{I}$, is shown in Fig. 4. In this subsection, we detail how the proposed GNN model extracts the key information from the locally estimated CSI and then designs the precoding vectors. Overall, GNN i contains L graph convolutional layers, denoted by $\{\text{GNN}_i^1, \text{GNN}_i^2, \dots, \text{GNN}_i^L\}$, one feed-forward layer (FL) and one normalization layer (NL). The output of each layer is used

Fig. 4. The structure of GNN i .

as the input of the next layer. The index set of the graph convolutional layers per GNN is denoted by $\mathcal{L} = \{1, 2, \dots, L\}$.

1) *Initial Input*: The initial input, i.e., the initial feature vector of $n_{i,k}$, is the estimated CSI between BS i and the user k , which is represented by

$$\mathbf{v}_{i,k}^0 = \left[\Re \left\{ \hat{\mathbf{h}}_{i,k,\mathcal{A}_i}^T \right\}, \Im \left\{ \hat{\mathbf{h}}_{i,k,\mathcal{A}_i}^T \right\} \right]^T \in \mathbb{R}^{2M \times 1}, \quad (11)$$

where $\Re \left\{ \hat{\mathbf{h}}_{i,k,\mathcal{A}_i}^T \right\}$ and $\Im \left\{ \hat{\mathbf{h}}_{i,k,\mathcal{A}_i}^T \right\}$ represent the real and imaginary parts of $\hat{\mathbf{h}}_{i,k,\mathcal{A}_i}$, respectively. This is consistent with the requirement of neural networks for real-valued inputs. Note that the perfect CSI is not available at the BSs due to the channel estimation errors.

2) *Graph Convolution Layer*: The graph convolutional layers serve as fundamental components of GNN, responsible for updating the node feature vectors. Taking GNN_i^l as an example, the process of updating the feature vector $\mathbf{v}_{i,k}$ of $n_{i,k}$ is shown in Fig. 5. The input of GNN_i^l first goes through an MLP, referred to as $\alpha_i^l(\cdot)$, which maps the previous feature vectors into a high-dimensional space, thereby capturing additional network topology information. This step can be formulated as follows

$$\mathbf{f}_{i,k}^l = \alpha_i^l \left(\mathbf{v}_{i,k}^{l-1} \right), \quad (12)$$

$$\mathbf{f}_{i,k'}^l = \alpha_i^l \left(\mathbf{v}_{i,k'}^{l-1} \right), \forall n_{i,k'} \in \mathcal{C}(n_{i,k}), \quad (13)$$

where $\mathcal{C}(n_{i,k}) = \left\{ n_{i,k'} \mid \forall k' \in \mathcal{K}, k' \neq k \right\}$ denotes the set of all neighbouring nodes of $n_{i,k}$. We adopt element-wise max function $\beta(\cdot)$ to aggregate the outputs of neighbouring nodes, which is expressed as

$$\mathbf{g}_{i,k}^l = \beta \left(\left\{ \mathbf{f}_{i,k'}^l \mid \forall n_{i,k'} \in \mathcal{C}(n_{i,k}) \right\} \right). \quad (14)$$

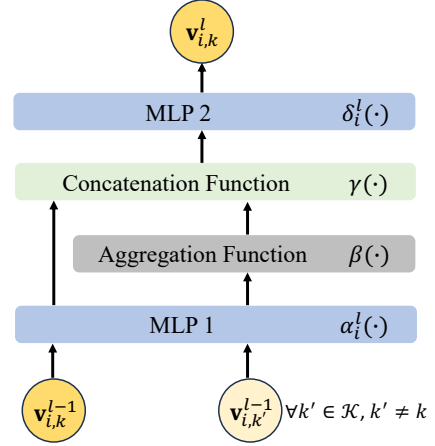
Then we concatenate the aggregated vector $\mathbf{g}_{i,k}^l$ with $\mathbf{f}_{i,k}^l$ and obtain the concatenated vector as follows

$$\mathbf{c}_{i,k}^l = \gamma \left(\mathbf{g}_{i,k}^l, \mathbf{f}_{i,k}^l \right), \quad (15)$$

where $\gamma(\cdot)$ denotes the concatenation function. Finally, an MLP, denoted by $\delta_i^l(\cdot)$, is employed to further extract information from $\mathbf{c}_{i,k}^l$ and output the new feature vector of $n_{i,k}$ at the l -th layer as follows

$$\mathbf{v}_{i,k}^l = \delta_i^l \left(\mathbf{c}_{i,k}^l \right). \quad (16)$$

It's worth noting that $\alpha_i^l(\cdot)$ and $\delta_i^l(\cdot)$ have the same hyper-parameters at all the user nodes, respectively. This reduces the number of hyper-parameters and enables faster convergence of the neural network's training.

Fig. 5. An illustration of graph convolutional layer GNN_i^l .

3) *Output*: After L graph convolutional layers, the feature vectors of user nodes have adequate information to design the corresponding precoding vectors. The feature vector of $n_{i,k}$ at the L -th layer, $\mathbf{v}_{i,k}^L$, is followed by a FL layer with $2M$ units that outputs a real-valued vector $\mathbf{v}'_{i,k} \in \mathbb{R}^{2M \times 1}$. We further convert $\mathbf{v}'_{i,k}$ to a complex-valued vector, which is given by

$$\mathbf{w}'_{i,k} = \left[\mathbf{v}'_{i,k} \right]_{1:M} + j \left[\mathbf{v}'_{i,k} \right]_{M+1:2M}. \quad (17)$$

Recall that each BS has a maximum transmit power P_{\max} . An NL is adopted to obtain the precoding matrix at BS i , \mathbf{W}_i , as follows

$$\mathbf{W}'_i = \left[\mathbf{w}'_{i,1}, \mathbf{w}'_{i,2}, \dots, \mathbf{w}'_{i,K} \right] \in \mathbb{R}^{M \times K}, \quad (18)$$

$$\mathbf{W}_i = \sqrt{P_{\max}} \frac{\mathbf{W}'_i}{\|\mathbf{W}'_i\|_F}. \quad (19)$$

Accordingly, the precoding vector of user k at BS i is given by $\mathbf{w}_{i,k} = [\mathbf{W}_i]_{:,k}$.

C. Offline Training and Online Deployment

The proposed distributed GNN-based precoding algorithm consists of two phases: offline training and online deployment, as shown in Fig. 6, where $\hat{\mathbf{H}}_{i,\mathcal{A}'_i} = \left[\hat{\mathbf{h}}_{i,1,\mathcal{A}'_i}, \hat{\mathbf{h}}_{i,2,\mathcal{A}'_i}, \dots, \hat{\mathbf{h}}_{i,K,\mathcal{A}'_i} \right] \in \mathbb{C}^{M \times K}$ is the estimated channel matrix between BS i and all the users under the randomly selected antenna subset \mathcal{A}'_i . The training phase occurs in the CPU in a centralized manner.

We adopt unsupervised learning to train the GNNs and directly use the opposite of the sum spectral efficiency of all the users in the cell-free MIMO network as the loss function, which is given by

$$\mathcal{L}_{\text{GNN}} = -\frac{1}{S} \sum_{s=1}^S \sum_{k \in \mathcal{K}} R_k(\mathcal{A}'_s, \mathbf{w}_{k,s}), \quad (20)$$

where S is the number of training samples, \mathcal{A}'_s is the global antenna subset for the s -th training sample following the random antenna selection strategy, and $\mathbf{w}_{k,s}$ is the precoding

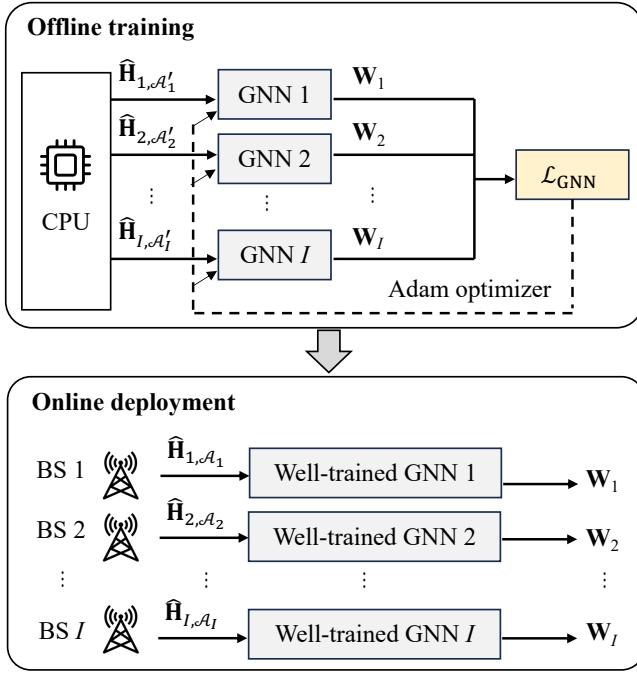


Fig. 6. Offline training and online deployment of the proposed distributed GNN-based algorithm.

vector from all BSs to user k determined by the GNNs for the s -th training sample. The Adam optimizer is adopted to minimize the loss function, i.e., maximize the sum spectral efficiency, and update the weight vectors of the GNNs. Since a large number of randomly selected antenna subsets are used in the training phase, the GNNs are capable of addressing an arbitrary given antenna selection strategy.

The online deployment phase is fully distributed, as shown in Fig. 6. Each BS initially acquires the pre-trained GNN models' weight parameters from the CPU. Subsequently, BS i employs its weight parameters to autonomously determine local precoding vectors based on a given active subset of antennas \mathcal{A}_i and its own locally estimated CSI $\hat{\mathbf{H}}_{i, \mathcal{A}_i}$.

IV. PROPOSED DISTRIBUTED CNN-BASED ANTENNA SELECTION

Recall that the number of the possible antenna selection strategies at all the BSs is $C = \prod_{i=1}^I C_i = \binom{N}{M}^I$, and thus antenna selection is a high-dimensional combinatorial optimization problem. It is difficult to get the solution within the channel coherence time using conventional schemes. Moreover, finding the optimal antenna selection strategy requires global CSI, which leads to a heavy fronthaul overhead. To address these challenges, we exploit advanced machine learning algorithms to learn the mapping relationship between the channel observations and the optimal antenna subsets. More specifically, we develop a distributed CNN-based antenna selection algorithm, where each BS uses a CNN to select a M -out-of- N subset of antennas only according to its locally estimated CSI.

Algorithm 1 Antenna selection dataset generation

Input: P_{\max}, I, N, M, K % System parameters

- 1: **for** $t = 1 : T$ **do**
 - 2: Generate channels $\mathbf{H} = [\mathbf{H}_1, \mathbf{H}_2, \dots, \mathbf{H}_I]$
 - 3: Generate estimated channels $\hat{\mathbf{H}} = [\hat{\mathbf{H}}_1, \hat{\mathbf{H}}_2, \dots, \hat{\mathbf{H}}_I]$
 - 4: $\mathbf{X}_i^t = [\Re \{ \hat{\mathbf{H}}_i \}; \Im \{ \hat{\mathbf{H}}_i \}]$ % Update the feature of training sample t in the antenna selection dataset of CNN i
 - 5: Initialize $\mathcal{A}_i, \forall i \in \mathcal{I}$, as the antenna subset with index 1 ($\mathcal{A}_i = \{1, 2, \dots, M\}$)
 - 6: Initialize $\mathbf{W}_i, \forall i \in \mathcal{I}$, using the well-trained GNNs
 - 7: $R_{\max} = 0$ % Initialize the maximum sum spectral efficiency
 - 8: **for** $i = 1 : I$ **do**
 - 9: **for** $j = 1 : \binom{N}{M}$ **do**
 - 10: Update \mathcal{A}_i as the antenna subset with index j
 - 11: Update \mathbf{W}_i using the well-trained GNN i
 - 12: Update $\sum_{k \in \mathcal{K}} R_k(\mathcal{A}, \mathbf{w}_k)$ according to (7)
 - 13: **if** $\sum_{k \in \mathcal{K}} R_k(\mathcal{A}, \mathbf{w}_k) > R_{\max}$ **then**
 - 14: $R_{\max} = \sum_{k \in \mathcal{K}} R_k(\mathcal{A}, \mathbf{w}_k)$
 - 15: $L_i^t = \mathcal{A}_i$ % Update the label of training sample t in the antenna selection dataset of CNN i
 - 16: **end if**
 - 17: **end for**
 - 18: **end for**
 - 19: **end for**
- Output:** $\{\mathbf{X}_i^t, L_i^t\}, i = 1, 2, \dots, I, t = 1, 2, \dots, T$

A. Dataset Generation

We deploy CNN i at BS i to select the optimal antenna subset \mathcal{A}_i . Since neural networks only support real-valued inputs, the input of CNN i is $\mathbf{X}_i = [\Re \{ \hat{\mathbf{H}}_i \}; \Im \{ \hat{\mathbf{H}}_i \}] \in \mathbb{R}^{2N \times K}$, where $\hat{\mathbf{H}}_i = [\hat{\mathbf{h}}_{i,1}, \hat{\mathbf{h}}_{i,2}, \dots, \hat{\mathbf{h}}_{i,K}] \in \mathbb{C}^{N \times K}$ is the estimated channel matrix between BS i and the users. In this paper, antenna selection is modeled as a classification problem, where CNN i selects an antenna subset from $C_i = \binom{N}{M}$ possible antenna selection strategies. The output of CNN i is the index of the selected antenna subset, denoted by L_i . Accordingly, training sample t in the antenna selection dataset of CNN i consists of two parts: feature, \mathbf{X}_i^t , and label, L_i^t , where \mathbf{X}_i^t is the real-valued input matrix at sample t and L_i^t is the index of the optimal antenna subset at BS i that maximizes the sum spectral efficiency.

The generation of antenna selection dataset is performed at the CPU as the calculation of the sum spectral efficiency requires global CSI. The exhaustive search algorithm iteratively evaluates all the possible antenna selection strategies and chooses the best one that maximizes the sum spectral efficiency. The number of searches is $C = \prod_{i=1}^I C_i = \binom{N}{M}^I$. Hence, the exhaustive search algorithm is not tractable for large numbers of antennas and BSs. To reduce the computational complexity, we propose a new iterative search (IS) algorithm that performs iterative searches segment by segment. Segment i is constructed by BS i and the users. In segment i , BS i iteratively searches $C_i = \binom{N}{M}$ possible antenna subsets

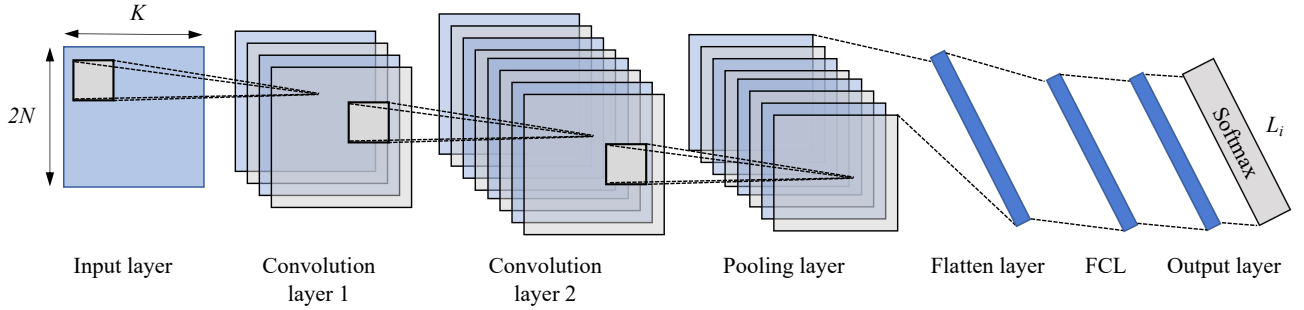


Fig. 7. The structure of CNN i .

and selects the best one that maximizes the sum spectral efficiency in (10). More specifically, the well-trained GNN i is applied to obtain the precoding matrix at BS i , i.e., \mathbf{W}_i , for each possible antenna subset. During the iterative searches in segment i , the antenna subsets in other BSs are fixed. The steps for generating the training samples are summarized in Algorithm 1, where T is the total number of samples in the dataset of each CNN. Overall, following the proposed IS algorithm, the size of the total search space reduces to $\binom{N}{M}I$, thereby greatly reducing the computational complexity. The numerical results in Section V show that the proposed IS algorithm can achieve a high sum spectral efficiency.

B. Structure of the Proposed CNN Models

We adopt CNN for antenna selection as it has a strong feature extraction ability and is good at processing grid-structured data. We deploy a CNN at each BS that takes the locally estimated CSI as input and outputs the index of the optimal antenna subset. The structure of the proposed CNN model at BS $i, \forall i \in \mathcal{I}$, is visualized in Fig. 7. To be specific, the CNN model consists of an input layer, 2 convolution layers, a pooling layer, a flatten layer, a fully-connected layer (FCL) and an output layer. The input of CNN i is the estimated local CSI at BS i , $\mathbf{X}_i = \left[\Re \{ \hat{\mathbf{H}}_i \}; \Im \{ \hat{\mathbf{H}}_i \} \right] \in \mathbb{R}^{2N \times K}$. Followed by the input layer, 2 convolution layers are used to extract features from the input with the well-known ReLU, i.e., $f(x) = \max(0, x)$, as activation function. A pooling layer is applied after the convolution layers to reduce the number of neural network parameters, improve the computational efficiency and reduce the risk of overfitting. The output of the pooling layer is then reshaped into a vector using a flattening layer. Subsequently, a FCL with ReLU as activation function is used between the flattening layer and the output layer to further extract information. Finally, the output layer consists of a $\binom{N}{M} \times 1$ FCL followed by a Softmax activation function given by

$$p_{z_i^j} = \frac{e^{z_i^j}}{\sum_{j=1}^J e^{z_i^j}}, \quad (21)$$

where z_i^j denotes the j -th output of the FCL at BS i , $J = \binom{N}{M}$, and $p_{z_i^j}$ is the probability of choosing the antenna subset with index j at BS i . The output vector of the Softmax classifier is denoted by $\mathbf{p}_i = \left[p_{z_i^1}, p_{z_i^2}, \dots, p_{z_i^J} \right]$, and the index of the

selected antenna subset is obtained as $L_i = \arg \max_j p_{z_i^j}$. Accordingly, \mathcal{A}_i is set to the antenna set with index L_i .

C. Offline Training of CNNs

The offline training of CNNs can be performed at the CPU or the BSs. If it is conducted at the BSs, the training dataset needs to be downloaded to the BSs. In contrast, if the training is performed at the CPU, the well-trained CNNs are downloaded to the BSs for online inference. The latter can significantly reduce the fronthaul overhead. Each CNN is independently trained using its own training dataset.

In the presence of training dataset, supervised learning is adopted to train the CNNs. We choose the cross-entropy loss function, which is widely-used in classification models. To this end, the labels in the dataset are converted into one-hot vectors. More specifically, the label of sample t in the dataset of CNN i , L_i^t , is converted into $\mathbf{d}_i^t \in \{0, 1\}^{\binom{N}{M} \times 1}$, where $[\mathbf{d}_i^t]_{L_i^t} = 1$ and $[\mathbf{d}_i^t]_l = 0, \forall l \neq L_i^t$. The cross-entropy loss function of CNN i is given by

$$\mathcal{L}_{\text{CNN}, i} = -\frac{1}{T} \sum_{t=1}^T \sum_{j=1}^J [\mathbf{d}_i^t]_j \log(p_{z_i^j}^t), \quad (22)$$

where T is the number of training samples and $p_{z_i^j}^t$ is the probability of choosing the antenna subset with index j at BS i for the t -th training sample.

D. Online Deployment of Joint Antenna Selection and Precoding

The online deployment of joint antenna selection and precoding is performed in a totally distributed manner, as shown in Fig. 8. Each BS downloads its own well-trained CNN and GNN from the CPU for local antenna selection and precoding design. After BS i obtains its locally estimated CSI, $\hat{\mathbf{H}}_i$, it selects antenna subset \mathcal{A}_i using the well-trained CNN i . Subsequently, the estimated CSI of the selected antenna subset, $\hat{\mathbf{H}}_{i, \mathcal{A}_i}$, is taken as input to the well-trained GNN i . Finally, the precoding matrix at BS i , \mathbf{W}_i , is obtained as the output of GNN i . Note that during the online deployment phase, both antenna selection and precoding require no information exchange among the BSs.

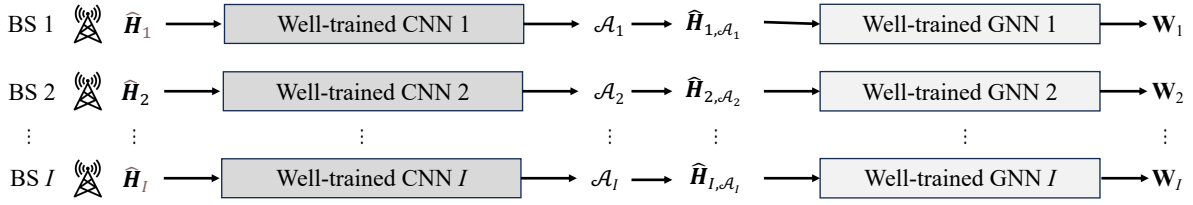


Fig. 8. Online deployment of joint antenna selection and precoding.

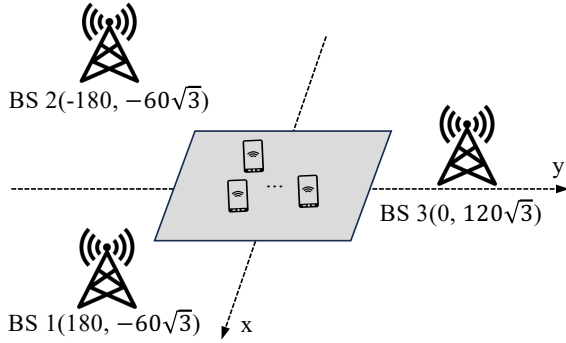


Fig. 9. Simulation setup for the cell-free MIMO network.

V. PERFORMANCE EVALUATION

This section presents the performance evaluation of our proposed joint CNN-based antenna selection and GNN-based precoding algorithm in comparison with the benchmark schemes.

A. Simulation Setup

As shown in Fig. 9, we consider a cell-free MIMO network consisting of three BSs and a number of users. The coordinates in meters of the three BSs are $(180, -60\sqrt{3})$, $(-180, -60\sqrt{3})$ and $(0, 120\sqrt{3})$, respectively. The users are uniformly and randomly distributed within a square area on the xy -plane with $x \in [-90, 90]$ m and $y \in [-90, 90]$ m. The large-scale path loss is given by

$$l(d) = l_0 - 10\alpha \log_{10} \left(\frac{d}{d_0} \right), \quad (23)$$

where $l_0 = -32.6$ dB represents the path loss at the reference distance, d_0 , which is set to 1 m, and $\alpha = 3.67$ represents the path loss exponent [34]. Since we focus on downlink transmission, we have $\tau_u = 0$. The noise power is computed by $\delta^2 = -174$ dBm/Hz + $10\log_{10}(W) + 7$ dB [24], where W is the channel bandwidth. The default simulation parameters are summarised in Table I unless otherwise stated.

B. GNN Setup

In this subsection, we present the network parameters of GNN i , $\forall i \in \mathcal{I}$, the structure of which has been shown in Fig. 4. We set the number of graph convolution layers to $L = 2$. In each graph convolution layer as shown in Fig. 5, the two MLPs, $\alpha_i^l(\cdot)$ and $\delta_i^l(\cdot)$, $\forall i \in \mathcal{I}, l \in \mathcal{L}$, share the same network architecture; each MLP has two layers with 800 and

TABLE I
DEFAULT SIMULATION PARAMETERS.

Parameters	Value
Channel bandwidth, W	20 MHz
Noise power, δ^2	-94 dBm
Coherence block length, τ_c	200
Pilot signal length, τ_p	10
Number of BSs, I	3
Maximum transmit power per BS, P_{\max}	20 dBm
Number of users, K	4
Number of antennas per BS, N	8
Number of active antennas per BS, M	5

400 neurons, respectively. Leaky ReLU is employed as the activation function, which is given by

$$g(x) = \begin{cases} x, & \text{if } x \geq 0 \\ \mu x, & \text{otherwise,} \end{cases} \quad (24)$$

where $\mu = 0.1$ is a slope to avoid the gradient being zero when the input is less than zero.

During the training stage, the GNNs are optimized with Adam optimizer using stochastic gradient descent (SGD). The training process lasts for 100 epochs. In each epoch, the model undergoes 100 iterations, where 600 groups of random user locations are sampled in each iteration. The initial learning rate is set to 0.001 and is decreased by a factor of 0.995 after every 100 iterations. The convergences of the proposed distributed GNN-based algorithm is shown in Fig. 10. We can see that the algorithm converges quickly under various system parameters. In particular, a satisfactory sum spectral efficiency can be achieved after 10 training epochs.

C. CNN Setup

The structure of CNN i , $\forall i \in \mathcal{I}$, has been shown in Fig. 7. The first convolution layer has 50 different 3×2 filters and the second convolution layer has 50 different 3×1 filters. A max pooling layer with a 2×2 filter is employed to down-sample the feature maps outputted by the convolution layers. The FCL between the flatten layer and the output layer has 128 neurons. The CNNs are trained for 50 epochs using the Adam optimizer with a batch size of 64.

Fig. 11 illustrates the impact of the number of training samples per CNN training dataset on the sum spectral efficiency. As can be observed, the sum spectral efficiency grows rapidly as the number of training samples increases from 10^3 to 10^4 . Then the growth trend slows down and the sum spectral efficiency saturates when the number of training

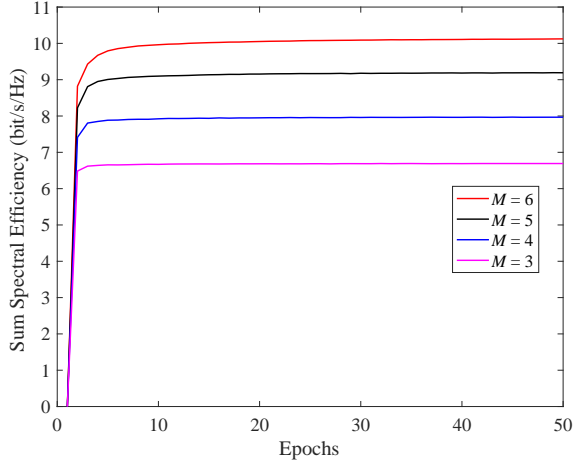


Fig. 10. Sum spectral efficiency versus training epochs.

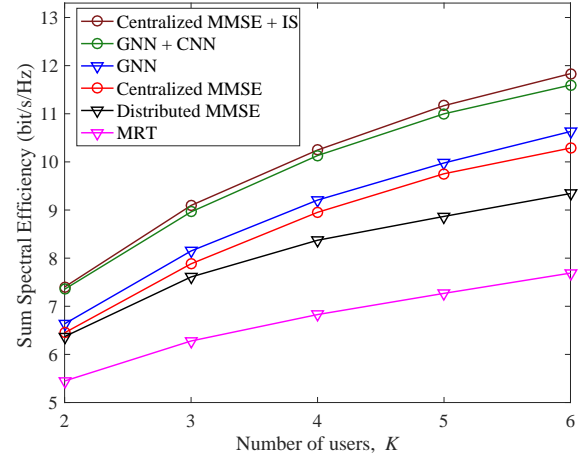


Fig. 12. Sum spectral efficiency versus the number of users.

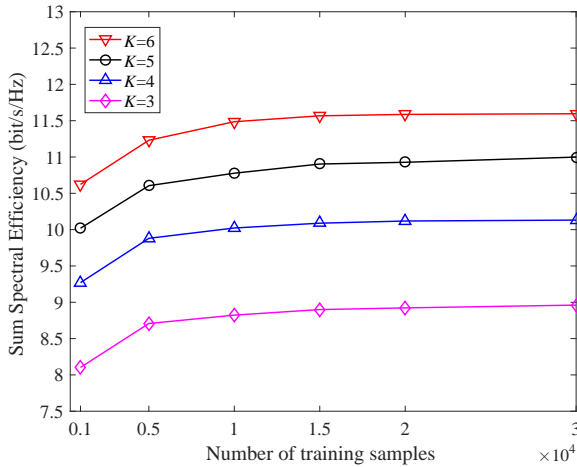


Fig. 11. The performance versus the size of training set.

samples reaches 3×10^4 . As such, we choose 3×10^4 as the size of the training dataset of each CNN.

D. Performance Comparison

This subsection demonstrates the superiority of the proposed joint CNN-based antenna selection and GNN-based precoding algorithm in comparison with the existing benchmark schemes. All the schemes are described as follows:

- **Centralized MMSE [35]:** Centralized MMSE precoding matrix is computed at the CPU by collecting the global CSI. Equal power allocation and random antenna selection strategy are adopted.
- **Centralized MMSE + IS:** Centralized MMSE precoding with equal power allocation is computed at the CPU using the global CSI. The proposed IS algorithm in Section IV-A is adopted for antenna selection.
- **Distributed MMSE:** Each BS computes its local MMSE precoding matrix using its local CSI. Equal power allocation and random antenna selection strategy are adopted.
- **MRT [4]:** MRT precoding focuses on maximizing the power of the desired signals. Equal power allocation

and random antenna selection strategy are adopted. The precoding matrix at each BS is the same as its local channel matrix, and thus no CSI exchange is required.

- **GNN:** The proposed distributed GNN-based precoding scheme with a random antenna selection strategy.
- **GNN + CNN:** The proposed distributed joint CNN-based antenna selection and GNN-based precoding algorithm.

In Fig. 12, we show the achievable sum spectral efficiency versus different numbers of users. We can see that the centralized MMSE + IS scheme achieves the highest sum spectral efficiency among the considered schemes. However, it requires the global CSI and has a high computational complexity. Notably, the proposed GNN + CNN scheme significantly outperforms the distributed benchmark schemes and achieves at least 97.83% sum spectral efficiency of the centralized MMSE + IS scheme for various numbers of users. This indicates that the proposed GNN + CNN scheme can achieve a sum spectral efficiency comparable to the centralized joint precoding and antenna selection scheme. In addition, we see that the centralized MMSE + IS and GNN + CNN schemes significantly outperform their counterparts without antenna selection, indicating the importance of antenna selection in improving the sum spectral efficiency.

Fig. 13 illustrates the sum spectral efficiency versus the maximum transmit power per BS. It is straightforward to see that the sum spectral efficiency monotonically increases with the maximum transmit power per BS. Moreover, the gap between the GNN + CNN scheme and the GNN scheme increases with the maximum transmit power per BS. For various values of maximum transmit power per BS, the proposed GNN + CNN scheme achieves a sum spectral efficiency close to the centralized MMSE + IS scheme. It is also observed that the proposed GNN scheme outperforms the centralized MMSE scheme in terms of the sum spectral efficiency. This is because the GNN scheme can achieve effective power allocation while the centralized MMSE scheme uses equal power allocation strategy. The MRT scheme achieves the lowest sum spectral efficiency among all considered schemes as it fails to suppress the inter-user interference.

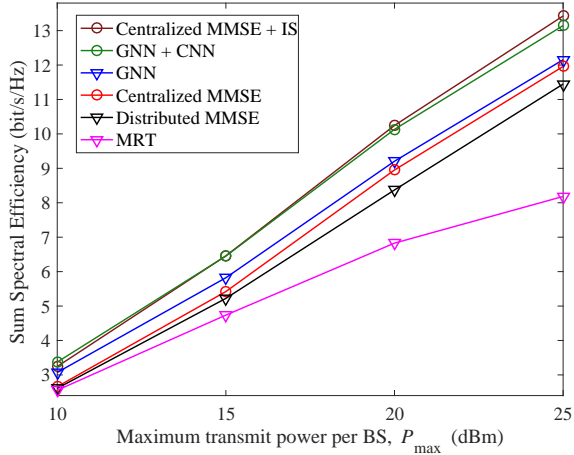


Fig. 13. Sum spectral efficiency versus the maximum transmit power.

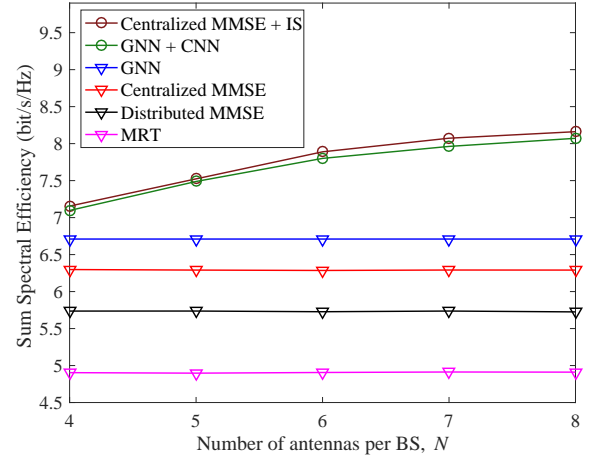


Fig. 15. Sum spectral efficiency versus the number of antennas per BS with $M = 3$.

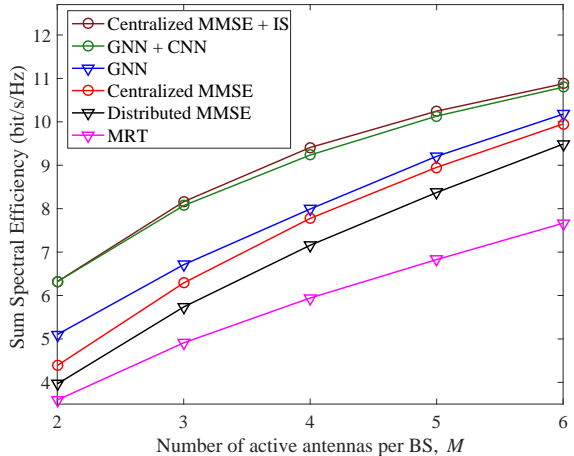


Fig. 14. Sum spectral efficiency versus the number of active antennas.

In Fig. 14, we present the sum spectral efficiency versus the number of active antennas per BS. We observe that for a given number of antennas, a higher sum spectral efficiency is achieved when more antennas are activated. It is interesting to see that the gap between the GNN + CNN scheme and the GNN scheme first increases and then decreases with the number of active antennas per BS. More specifically, the gap in bit/s/Hz first increases from 1.28 ($M=2$) to 1.43 ($M=3$), and then decreases to 0.65 ($M=6$). Generally, the gain of antenna selection in terms of sum spectral efficiency is more significant when less antennas are activated. This demonstrates the importance of antenna selection for a small number of active antennas per BS.

In Fig. 15, we show the impact of the number of antennas per BS on the sum spectral efficiency. In particular, the centralized MMSE, distributed MMSE, MRT and GNN schemes adopt the random antenna selection strategy, and thus the sum spectral efficiency of these schemes remains unchanged with the number of antennas per BS. In contrast, for a given number of active antennas per BS, the GNN + CNN and centralized MMSE + IS schemes can achieve a higher sum spectral

efficiency when the number of antennas per BS increases. This indicates the necessity of antenna selection when each BS is equipped with a large number of antennas.

Overall, we can conclude from Fig. 12-15 that the proposed distributed GNN-based precoding scheme is effective in achieving a high sum spectral efficiency. In addition, the proposed fully distributed joint GNN-based precoding and CNN-based antenna selection scheme achieves a sum spectral efficiency comparable to its centralized counterpart for various system parameters.

In Table II, we present the sum spectral efficiency, computational time, and information exchange of the proposed GNN + CNN scheme and the centralized MMSE + IS scheme. The sum spectral efficiency and computational time are averaged over 1000 independent channel realizations. We implement all the considered schemes using Python 3.8 on a laptop with a 4 core Intel Core i7 CPU with 2.2 GHz base frequency and 16 GB memory. The information exchange consists of CSI transmitted from the BSs to the CPU and precoding vectors conveyed from the CPU to the BSs in a coherence block. We see that compared to the centralized MMSE + IS scheme, the proposed GNN + CNN scheme achieves 98.8% sum spectral efficiency with only 0.25% computational time. Moreover, the proposed GNN + CNN scheme is fully distributed, requiring no information exchange. Therefore, the proposed GNN + CNN scheme can achieve real-time processing and alleviate the fronthaul overhead. Although the computational complexity is slightly higher than the baseline schemes without antenna selection, the proposed GNN + CNN scheme provides significant sum spectral efficiency gain.

VI. CONCLUSION

In this paper, the joint design of antenna selection and precoding in the downlink of a cell-free MIMO network has been addressed. We have formulated a sum spectral efficiency maximum problem, considering realistic pilot-aided CSI acquisition. A novel fully distributed machine learning algorithm has been proposed to maximize the sum spectral

TABLE II
COMPARISON OF SUM SPECTRAL EFFICIENCY, COMPUTATIONAL TIME, AND INFORMATION EXCHANGE.

Algorithm	Sum spectral efficiency (bit/s/Hz)	Computational time (ms)	Information exchange (complex scalars)
Centralized MMSE + IS	10.25	240.89	$INK + IMK$
GNN + CNN	10.13	0.6	0
Centralized MMSE	8.95	0.34	$2IMK$
Distributed MMSE	8.37	0.35	0

efficiency. More specifically, each BS deploys a CNN for antenna selection and a GNN for precoding design using only locally estimated CSI as input, and so alleviating the fronthaul overhead. Unsupervised learning has been used to train the GNNs, bypassing the time-consuming phase of dataset generation. The proposed distributed machine learning algorithm effectively finds the mapping relationship between the local domain input and the desired antenna selection as well as precoding design. Simulation results illustrate that the proposed distributed machine learning algorithm achieves a sum spectral efficiency close to its centralized counterpart with a much less computational time. In the future, it will be of interest to investigate joint antenna selection and user association in a user-centric cell-free MIMO network.

REFERENCES

- [1] C.-X. Wang, X. You, X. Gao, X. Zhu, Z. Li, C. Zhang, H. Wang, Y. Huang, Y. Chen, H. Haas *et al.*, "On the road to 6G: Visions, requirements, key technologies and testbeds," *IEEE Commun. Surv. Tutor.*, 2023.
- [2] S. Parkvall, E. Dahlman, A. Furuskar, and M. Frenne, "NR: The new 5G radio access technology," *IEEE Commun. Mag.*, vol. 1, no. 4, pp. 24–30, 2017.
- [3] C. Chen, J. Zhang, X. Chu, and J. Zhang, "On the deployment of small cells in 3D HetNets with multi-antenna base stations," *IEEE Trans. Wirel. Commun.*, vol. 21, no. 11, pp. 9761–9774, 2022.
- [4] H. Q. Ngo, A. Ashikhmin, H. Yang, E. G. Larsson, and T. L. Marzetta, "Cell-free massive MIMO versus small cells," *IEEE Trans. Wireless Commun.*, vol. 16, no. 3, pp. 1834–1850, Mar. 2017.
- [5] A. Burr, M. Bashar, and D. Maryopi, "Ultra-dense radio access networks for smart cities: Cloud-RAN, fog-RAN and "cell-free" massive MIMO," *arXiv preprint arXiv:1811.11077*, 2018.
- [6] H. Q. Ngo, L.-N. Tran, T. Q. Duong, M. Matthaiou, and E. G. Larsson, "On the total energy efficiency of cell-free massive MIMO," *IEEE trans. green commun. netw.*, vol. 2, no. 1, pp. 25–39, 2017.
- [7] R. W. Heath and A. Paulraj, "Antenna selection for spatial multiplexing systems based on minimum error rate," in *Proc. IEEE Int. Conf. Commun.*, Jun. 2001, pp. 2276–2280.
- [8] D. López-Pérez, A. De Domenico, N. Piovesan, G. Xinli, H. Bao, S. Qitao, and M. Debbah, "A survey on 5G radio access network energy efficiency: Massive MIMO, lean carrier design, sleep modes, and machine learning," *IEEE Commun. Surv. Tutor.*, vol. 24, no. 1, pp. 653–697, 2022.
- [9] X. Gao, O. Edfors, F. Tufvesson, and E. G. Larsson, "Massive MIMO in real propagation environments: Do all antennas contribute equally?" *IEEE Trans. Commun.*, vol. 63, no. 11, pp. 3917–3928, 2015.
- [10] B. Makki, A. Ide, T. Svensson, T. Eriksson, and M.-S. Alouini, "A genetic algorithm-based antenna selection approach for large-but-finite MIMO networks," *IEEE Trans. Veh. Technol.*, vol. 66, no. 7, pp. 6591–6595, 2016.
- [11] M. Guo and M. C. Gursoy, "Statistical learning based joint antenna selection and user scheduling for single-cell massive MIMO systems," *IEEE trans. green commun. netw.*, vol. 5, no. 1, pp. 471–483, 2020.
- [12] S. Wang, M. Zhu, Z. Li, L. Yang, C.-X. Wang, and R. Ruby, "Antenna selection strategies for massive MIMO systems with limited-resolution ADCs/DACs," *IEEE Trans. Wireless Commun.*, 2023.
- [13] P. Zhu, Z. Sheng, J. Bao, and J. Li, "Antenna selection for full-duplex distributed massive MIMO via the elite preservation genetic algorithm," *IEEE Commun. Lett.*, vol. 26, no. 4, pp. 922–926, 2022.
- [14] J. C. Marinello, T. Abrão, A. Amiri, E. De Carvalho, and P. Popovski, "Antenna selection for improving energy efficiency in XL-MIMO systems," *IEEE Trans. Veh. Technol.*, vol. 69, no. 11, pp. 13305–13318, 2020.
- [15] O. Elijah, S. K. A. Rahim, W. K. New, C. Y. Leow, K. Cumanan, and T. K. Geok, "Intelligent massive MIMO systems for beyond 5G networks: An overview and future trends," *IEEE Access*, vol. 10, pp. 102532–102563, 2022.
- [16] H. Hellström, J. M. B. da Silva Jr, M. M. Amiri, M. Chen, V. Fodor, H. V. Poor, C. Fischione *et al.*, "Wireless for machine learning: A survey," *Foundations and Trends® in Signal Processing*, vol. 15, no. 4, pp. 290–399, 2022.
- [17] H. Guo and V. K. Lau, "Robust deep learning for uplink channel estimation in cellular network under inter-cell interference," *IEEE J. Sel. Areas Commun.*, 2023.
- [18] E. Balevi, A. Doshi, and J. G. Andrews, "Massive MIMO channel estimation with an untrained deep neural network," *IEEE Trans. Wireless Commun.*, vol. 19, no. 3, pp. 2079–2090, 2020.
- [19] T. Jiang, H. V. Cheng, and W. Yu, "Learning to reflect and to beamform for intelligent reflecting surface with implicit channel estimation," *IEEE J. Sel. Areas Commun.*, vol. 39, no. 7, pp. 1931–1945, 2021.
- [20] C. Chen, S. Xu, J. Zhang, and J. Zhang, "A distributed machine learning-based approach for IRS-enhanced cell-free MIMO networks," *IEEE Trans. Wireless Commun.*, 2023.
- [21] Y. Chen, W. Xia, J. Zhang, and Y. Zhu, "Joint learning of channel estimation and beamforming for cell-free massive MIMO systems," *IEEE Wirel. Commun. Lett.*, 2024.
- [22] N. Ghiasi, S. Mashhadi, S. Farahmand, S. M. Razavizadeh, and I. Lee, "Energy efficient ap selection for cell-free massive MIMO systems: Deep reinforcement learning approach," *IEEE trans. green commun. netw.*, vol. 7, no. 1, pp. 29–41, 2022.
- [23] C. D'Andrea, A. Zappone, S. Buzzi, and M. Debbah, "Uplink power control in cell-free massive MIMO via deep learning," in *2019 IEEE 8th International workshop on computational advances in multi-sensor adaptive processing (CAMSAP)*. IEEE, 2019, pp. 554–558.
- [24] M. Zaher, Ö. T. Demir, E. Björnson, and M. Petrova, "Learning-based downlink power allocation in cell-free massive MIMO systems," *IEEE Trans. Wireless Commun.*, vol. 22, no. 1, pp. 174–188, 2022.
- [25] J. Joung, "Machine learning-based antenna selection in wireless communications," *IEEE Commun. Lett.*, vol. 20, no. 11, pp. 2241–2244, 2016.
- [26] S. Geggel, C. Goztepe, and G. K. Kurt, "Transmit antenna selection for large-scale MIMO GSM with machine learning," *IEEE Wirel. Commun. Lett.*, vol. 9, no. 1, pp. 113–116, 2019.
- [27] T. X. Vu, S. Chatzinotas, V.-D. Nguyen, D. T. Hoang, D. N. Nguyen, M. Di Renzo, and B. Ottersten, "Machine learning-enabled joint antenna selection and precoding design: From offline complexity to online performance," *IEEE Trans. Wireless Commun.*, vol. 20, no. 6, pp. 3710–3722, 2021.
- [28] A. M. Elbir and K. V. Mishra, "Joint antenna selection and hybrid beamformer design using unquantized and quantized deep learning networks," *IEEE Trans. Wireless Commun.*, vol. 19, no. 3, pp. 1677–1688, Mar. 2020.
- [29] X. Chai, H. Gao, J. Sun, X. Su, T. Lv, and J. Zeng, "Reinforcement learning based antenna selection in user-centric massive MIMO," in *2020 IEEE 91st Vehicular Technology Conference (VTC2020-Spring)*. IEEE, 2020, pp. 1–6.
- [30] E. Björnson, L. Sanguinetti, J. Hoydis, and M. Debbah, "Optimal design of energy-efficient multi-user MIMO systems: Is massive MIMO the answer?" *IEEE Trans. Wirel. Commun.*, vol. 14, no. 6, pp. 3059–3075, 2015.
- [31] H. A. Ammar, R. Adve, S. Shahbazpanahi, G. Boudreau, and K. V. Srinivas, "Downlink resource allocation in multiuser cell-free MIMO networks with user-centric clustering," *IEEE Trans. Wireless Commun.*, vol. 21, no. 3, pp. 1482–1497, 2021.

- [32] J. Jose, A. Ashikhmin, T. L. Marzetta, and S. Vishwanath, "Pilot contamination and precoding in multi-cell TDD systems," *IEEE Trans. Wireless Commun.*, vol. 10, no. 8, pp. 2640–2651, 2011.
- [33] J. Gilmer, S. S. Schoenholz, P. F. Riley, O. Vinyals, and G. E. Dahl, "Neural message passing for quantum chemistry," in *Proc. Int. Conf. Mach. Learn. (ICML)*, 2017, pp. 1263–1272.
- [34] C. Chen, J. Zhang, T. Lu, M. Sandell, and L. Chen, "Secret key generation for IRS-assisted multi-antenna systems: A machine learning-based approach," *IEEE Trans. Inf. Forensics Secur.*, vol. 19, pp. 1086–1098, 2024.
- [35] E. Björnson and L. Sanguinetti, "Making cell-free massive MIMO competitive with MMSE processing and centralized implementation," *IEEE Trans. Wireless Commun.*, vol. 19, no. 1, pp. 77–90, 2019.